Thermal and Electrical Conduction in Ultrathin Metallic Films: 7 nm down to Sub-Nanometer Thickness

Huan Lin, Shen Xu, Xinwei Wang, and Ning Mei*

***F**or ultrathin metallic films (e.g., less than 5 nm), no knowledge is yet available on how electron scattering at surface and grain boundaries reduces the electrical and thermal transport. The thermal and electrical conduction of metallic films is characterized down to 0.6 nm average thickness. The electrical and thermal conductivities of 0.6 nm Ir film are reduced by 82% and 50% from the respective bulk values. The Lorenz number is measured as 7.08×10^{-8} W Ω K^{-2}, almost a twofold increase of the bulk value. The Mayadas-Shatzkes model is used to interpret the experimental results and reveals very strong electron reflection (>90%) at grain boundaries.*

1. Introduction

Metallic thin films are widely used as interconnects in the semiconductor industries so the thermal and electrical properties of metallic thin-film structures have attracted considerable attention. In particular, the electrical-transport properties of nanometer-thick metallic films have been investigated intensively in recent years.[1,2] In contrast to the extensive studies of electrical transport, only a few experimental investigations of in-plane thermal conductivity of nanometer-thick metallic films have been reported,[3–6] in part because the thermal transport in nanometer-thick metallic films in the in-plane direction is very difficult to characterize, especially for film thicknesses of less than 5 nm. When the size of a metal interconnect is comparable to the electron mean free path, electron transport is dominated by scattering at the metal–dielectric interface, which can reduce the electrical and thermal conductivities to less than half of the bulk value.[7–11] Several experimental studies investigated either the thermal conductivity or the electrical conductivity and used the electrical–thermal analogy to determine the other value.[12] For bulk materials we can use the Wiedemann-Franz (WF) law to calculate the thermal conductivity, by using an analogy approach between charge transport and heat transport. However, the WF law has not been validated for special metals, such as nanocrystalline films, and the Lorenz numbers of nanofilms are very different from their corresponding bulk values.[4,13–16] Yoneoka et al.[3] measured the average Lorenz number to be 3.82×10^{-8}, 2.79×10^{-8}, and 2.99×10^{-8} W Ω K^{-2} for 7.3-, 9.8-, and 12.1-nm Pt films, respectively. Experimental results of Zhang and co-workers[16,17] showed that the Lorenz numbers are around 7.0×10^{-8} and 5.0×10^{-8} W Ω K^{-2} for 21–37-nm and 53-nm thick polycrystalline Au films, respectively. Zhang and co-workers[4,5,17] found that the Lorenz numbers for 15-, 28-, and 48-nm Pt nanofilms are several times larger than the bulk value. Calculations by Ou et al.[18] revealed that the Lorenz number of a 180-nm nickel nanowire is a little higher than the bulk value. It should be pointed out that for very thin films, 5 nm or thinner, no research has been done on the heat conduction and Lorenz number, while such research is very critical to understand the role of electrons in thermal and electrical conduction with strong interface scattering.

In this work we develop a robust and advanced technique to characterize the thermal and electrical transport in nanoscale metallic films simultaneously and characterize the Lorenz number more precisely. We study the electrical and thermal conductivities of polycrystalline iridium (Ir) films with an average thickness of 0.6–7 nm. The experimental results are interpreted using Mayadas and Shatzkes (MS) theory[19,20] to understand the electron scattering at the grain boundary.

H. Lin, S. Xu, Prof. X. Wang
2010 Black Engineering Building
Department of Mechanical Engineering
Iowa State University
Ames, Iowa 50011, USA
Phone: (515) 294-2085, Fax: (515) 294-3261
E-mail: xwang3@iastate.edu
H. Lin, N. Mei
College of Engineering
Ocean University of China
Qingdao, Shandong, 266100, PR China

DOI: 10.1002/smll.201202877

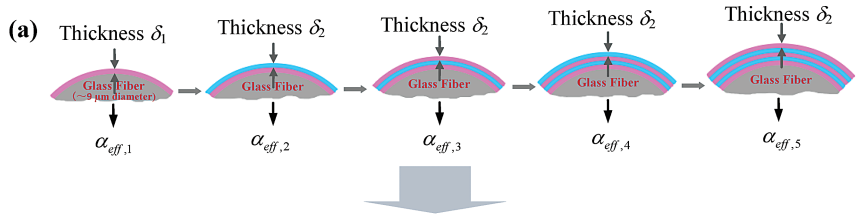

From the α_{eff} variation against the number of metallic coating layers and electrical conductance (R^{-1}) to determine the Lorenz number, thermal conductivity, and electrical conductivity.

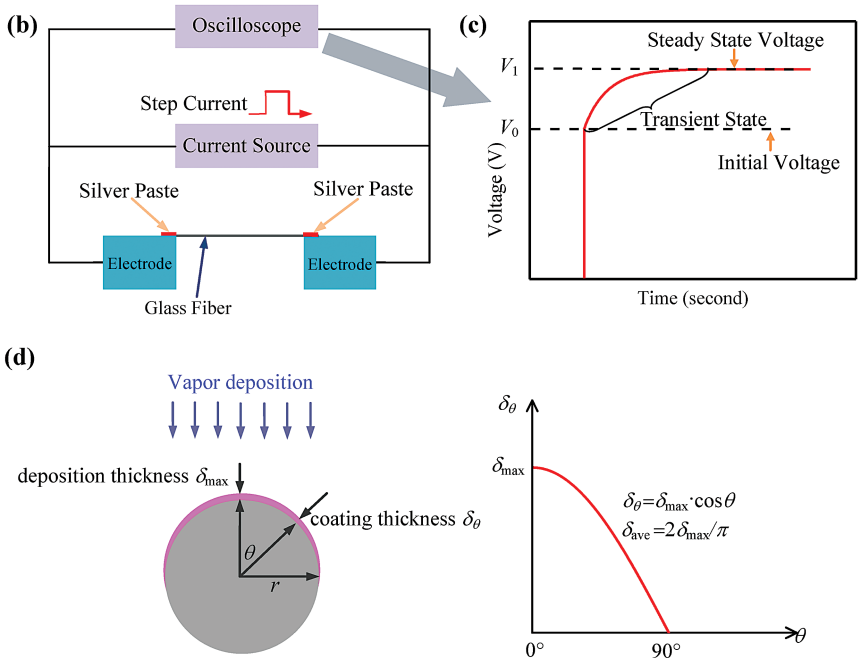

Figure 1. a) Schematic of the cross-section of glass fiber coated with different layers of nanometer films. Different colors on the glass fiber represent different layers of the metallic film. By fitting the TET state of the same glass fiber with different numbers of metallic coating layers we can determine their effective thermal diffusivities. These data such as resistance, number of metallic coating layers, and effective thermal diffusivity in all the TET experiments can be used to determine the Lorenz number, thermal conductivity, and electrical conductivity of the metallic film layer. b) Schematic of the experimental principle and the step current provided for the TET technique. c) Methodology to determine the thermophysical properties based on the experimental *V*–*t* profile (not to scale). d) Profile of the film thickness, and definition of thickness δ_{max} and δ_θ.

2. Results

In this work, a differential technology is developed to achieve novel capacity of thermal diffusivity/conductivity measurement for ultrathin metallic films. In this method, as shown in **Figure 1**a, a low-dimensional and low thermal conductivity material (micro-glass fiber in this work) is used as the support for the ultrathin metallic film. First of all, the glass fiber is coated with one metallic film/layer of thickness δ_1, and the effective thermal diffusivity of the glass fiber–metallic film system (in the axial direction) is measured as $\alpha_{eff,1}$. Then the same sample is coated with a second metallic layer of thickness δ_2, and the sample's thermal diffusivity is measured again as $\alpha_{eff,2}$. The differential/incremental of the thermal diffusivity induced by the second metallic layer is $\Delta\alpha_{eff} = \alpha_{eff,1}-\alpha_{eff,2}$. This thermal diffusivity differential is directly related to the thermal conductivity of the second metallic layer of thickness δ_2, and other parameters of the sample, like the glass fiber's diameter, thermal conductivity, and ρc_p (the effective density and specific heat of the glass fiber). A physical model is developed in this work to determine the thermal conductivity of the metallic layer based on $\Delta\alpha_{eff}$. For thermal characterization of a one-dimensional material, in our technology the material has to be electrically conductive. Therefore, we need to coat the glass fiber with the first metallic layer of thickness δ_1 to achieve the measurement. Theoretically, to measure the thermal conductivity of the second metallic layer of thickness δ_2, we need to coat only one second layer (δ_2 thickness) and do the measurement for $\alpha_{eff,2}$. To improve measurement accuracy and significantly suppress experimental uncertainty, we will repeat the addition of a metallic layer of thickness δ_2 and measure the corresponding thermal diffusivity $\alpha_{eff,n}$. Finally, we will establish a relationship between $\alpha_{eff,n}$ and the number (n) of the metallic layer (δ_2 thickness). Then based on the theoretical model, the thermal conductivity of a single metallic layer of thickness δ_2 can be determined precisely. Also determined at the same time are the Lorenz number (L_{Lorenz}) and electrical conductivity (σ) of a single metallic

NANO MICRO small

layer of thickness δ_2. In the methodology, the first metallic layer (δ_1 thickness) is intended to make the sample electrically conductive, so its thickness can be the same or different from δ_2. When measuring very thin metallic layers (δ_2 is only a few nanometers or thinner), the first layer of thickness δ_1 also plays a role to ensure electrical stability of the sample. In this situation, δ_1 usually is much thicker than δ_2. During each round of experiment, a layer of the same thickness δ_2 is deposited on top of the previous one. Since each deposited film layer has the same thickness and is under the exact same conditions during deposition, it is physically reasonable to assume they have the same electrical and thermal conductivities and ρc_p. This assumption will be validated and discussed later based on the measurement results.

The transient electro-thermal (TET) technique[21] developed in our laboratory is used in this work to measure the thermal diffusivity of the metallic-layer-covered micro-glass fiber. A schematic of the TET technology is presented in Figure 1b. The to-be-measured wire is suspended between two aluminum electrodes, and housed in a vacuum chamber. During thermal characterization, a step DC current is fed through the wire to generate electric heat, and the step DC current is also used to probe the temperature evolution of the sample. A typical V–t profile recorded by the oscilloscope is shown in Figure 1c. After the normalized temperature rise (T^*_{exp}) of the sample is obtained experimentally, different trial values of thermal diffusivity of the sample (α) are used to calculate the theoretical temperature rise based on the physical model and to fit the experimental results (T^*_{exp}). The value giving the best fit of T^*_{exp} is taken as the thermal diffusivity of the sample. Details of the measurement principle and capacity are given in the Experimental Section.

The measured thermal diffusivity (α_{eff}) is an effective value combining both effects of the glass fiber and metallic coating. The thermal transport effect caused by the coated layer can be described using the Lorenz number without increasing uncertainty. If there is only one metallic layer on top of the glass fiber, the measured effective thermal diffusivity is related to the thermal transport in the glass wire and metallic coating as[21] $\alpha_{eff} = \alpha_w + L_{Lorenz}TL/(RA_w\rho c_p)$, where L_{Lorenz} is the Lorenz number, A_w the cross-sectional area of bare wire, and α_w the real thermal diffusivity of the glass fiber itself. T and R are average temperature and resistance of the glass fiber during the TET experiment. ρ and c_p are the effective density and specific heat of the glass fiber. Herein, we will use this relation to determine the Lorenz number of metallic films. Details are given in the case studies for multilayer metallic films below.

The glass fiber's diameter and density are determined to be 9.17 ± 0.54 μm and 2070 ± 121 kg m^{-3}. Herein, the thermal and electrical conduction in ultrathin Ir films are studied. The thicknesses δ_{max} (shown in Figure 1d) of the Ir films are 1, 2.8, 7.7, 10, and 11 nm. Selection of the metallic films is based on the availability of the coating machines accessible to our laboratory, not limited by the measurement technique itself. Ultrathin metallic films of other materials can also be studied and such study will be carried out in the near future. The profile of the metallic layers on the glass fiber is illustrated in Figure 1d. Details about film deposition and thickness measurement are given in the Experimental Section.

2.1. Thermal and Electrical Conduction in δ_{ave} = 6.4-nm Thick Ir Film

During this Ir coating deposition, the quartz crystal microbalance gives a reading of 10 nm, meaning δ_{max} = 10 nm for the film on the glass fiber, and the corresponding δ_{ave} is 6.4 nm. First we coat one glass fiber (401 μm long) with δ_{max} = 10 nm Ir and do the TET experiment. After that we add another δ_{max} = 10 nm Ir layer on the same glass fiber and repeat the TET experiment. In all, we do the TET experiment five times with the same glass fiber coated with δ_{max} = 10 nm Ir layers. Five different effective thermal diffusivity values are obtained. The upper left inset in **Figure 2**a shows the normalized temperature rise with the theoretical fitting to determine the effective thermal diffusivity of the sample. From this inset, we can see that with five Ir layers, the normalized temperature of the sample goes up faster than that with single Ir layer, meaning that the effective thermal diffusivity of the glass fiber with five Ir layers is bigger than that with a single Ir layer. By fitting, the effective thermal diffusivities are determined to be 9.28×10^{-7} and 7.14×10^{-7} m^2 s^{-1} for the same glass fiber with five Ir layers and just one Ir layer.

After five repeats of the TET experiment, we get five different measured thermal diffusivities varying with the inverse of electrical resistance. It can be seen from $\alpha_{eff} = \alpha + L_{Lorenz}TL/(RA_w\rho c_p)$ that the effective thermal diffusivity (α_{eff}) changes with the inverse of resistance (R^{-1}) linearly and the slope of the fitting line is $L_{Lorenz}TL/A_w\rho c_p$. Figure 2a shows the linear fit of effective thermal diffusivity change against R^{-1}. The measured thermal diffusivity (α_{eff}) is an effective value that combines effects of both the glass fiber and the Ir coating. By linear fitting of data points and extending the fitting line to the y axis we can get an intersection point between the y axis and the fitting line as shown in Figure 2a. The value of this point is 6.35×10^{-7} m^2 s^{-1}, which is the real thermal diffusivity of the glass fiber because at this point ($R^{-1} \to \infty$) there is no Ir coating. The thermal conductivity of the glass fiber is calculated as 0.98 W m^{-1} K^{-1} according to the expression of thermal diffusivity, $\alpha = k/\rho c_p$. The glass fiber measured in this work has a lower density (2070 kg m^{-3}) than that (2220 kg m^{-3})[22] of bulk glass, a fact that is largely attributed to defects (e.g., cavities) induced during fiber spinning. We could not find a reported value for thermal conductivity of single micron-thick glass fibers for comparison, so bulk glass is used here for approximate comparison and discussion. From Maxwell's equation for the effective thermal conductivity of the mixture, $k_e/k_f = 1 + 3(\xi\text{-}1)\varphi/[(\xi\text{+}2)\text{-}(\xi\text{-}1)\varphi]$,[23] where ξ is the ratio of thermal conductivity of air to that of bulk glass, k_f is the thermal conductivity of bulk glass (1.38 W m^{-1} K^{-1}), and φ = 1–2070/2220 = 6.76%, k_e is calculated at 1.24 W m^{-1} K^{-1}. This value only considers the effect of air cavity in the glass fiber. Since the glass fiber is very thin (<10 μm), and the porosity level is low (6.76%), it is highly possible that the air cavities in the fiber could be very fine, maybe on the nanometer scale. Such extremely small cavities will give extra phonon scattering in the glass fiber, leading to further thermal conductivity reduction. The above comparison is based on the thermal conductivity of bulk glass (fused silica). Glass fibers are fabricated using a different process from the bulk glass,

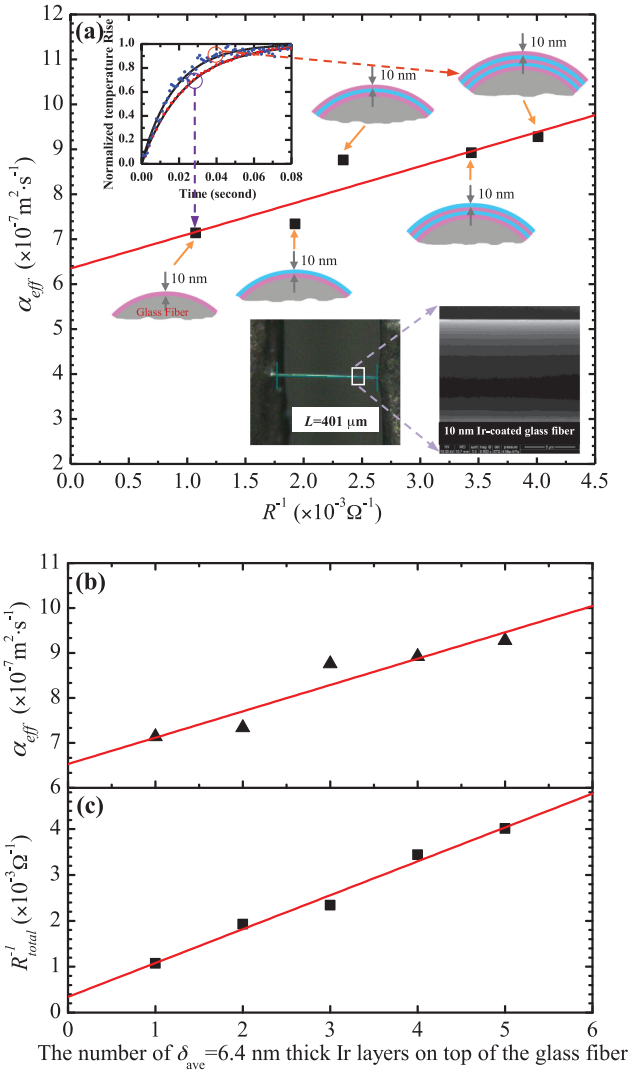

Figure 2. a) Variation of the effective thermal diffusivity of an Ir-coated glass fiber (401 μm long) against the inverse of the electrical resistance for 6.4-nm Ir layers coated on the glass fiber. The solid line is a linear fit of the five data points. The upper left inset is a comparison between the theoretical fitting and experimental data for the normalized temperature rise for a glass fiber coated with Ir. The blue and red dots are experimental data of the glass fiber coated with five Ir layers and with a single Ir layer, respectively. The solid lines are theoretical fits of the experimental data. The lower two insets show the glass fiber connected between two electrodes and a scanning electron microscope (SEM) image of Ir coated on a glass fiber; it shows that the glass fiber surface is very smooth. b) Linear fitting curve of effective thermal diffusivity change with the number of Ir layers on top of the glass fiber. c) Linear fitting curve of resistance change with the number of Ir layers on top of the glass fiber. Solid lines are linear fits of the experimental data.

and experience much faster cooling and solidification due to their very small thickness. It is expected that glass fibers will have higher structural disorder than fused silica, which results in a lower thermal conductivity than that of bulk fused silica. Also the additives/impurities in this glass fiber induced during fabrication will induce extra phonon scattering and reduce its thermal conductivity. In conclusion, we do not feel the glass fiber will share the same thermal conductivity as bulk fused silica, and the measured thermal diffusivity/conductivity of the glass fiber in this work is accurate considering all the factors discussed above.

The slope (ψ) of the fitting line is determined to be 7.85×10^{-5} m^2 s^{-1} Ω (shown in Figure 2a). In the five TET experiments the electrical current is controlled in a range of 264–614 μA to have a visible, but not too great, voltage rise. The temperature rise of the transient stage is estimated to be around 16 K. For Lorenz number calculation, an average temperature during the transient state (313 K) is used. With this detailed information we determine the Lorenz number of 6.4-nm thick Ir layer as 6.15×10^{-8} W Ω K^{-2}, according to $L_{\text{Lorenz}} = A_w \rho c_p \psi / TL$.

In our experiment, the measured thermal diffusivity has a combined contribution from the glass fiber and the Ir layers. The contribution is proportional to their areas. The effective thermal diffusivity of the whole sample can also be determined as Equation (1),

$$\alpha_{\text{eff}} = \frac{A_c k_c + A_w k_w}{A_c (\rho c_p)_c + A_w (\rho c_p)_w} \quad (1)$$

where k is thermal conductivity, and A is the cross-sectional area, while subscripts c and w indicate the Ir layers and bare glass fiber, respectively. By introducing $\gamma = A_c/A_w$, then Equation (1) is written as Equation (2)

$$\alpha_{eff} = \alpha_w + \frac{4 \cdot n \cdot \delta_{\max}}{\pi D (\rho c_p)_w} \left[k_c - \alpha_w (\rho c_p)_c \right] \quad (2)$$

where α_w is the thermal diffusivity of glass fiber, and is a constant value. In Equation (2), it is clear that α_{eff} changes with n linearly and its slope is $4\delta_{\max}[k_c - \alpha_w (\rho c_p)_c] / \pi D (\rho c_p)_w$. After doing five different TET experiments with the same conditions but different Ir layer numbers, five groups of (α_{eff}, n) are obtained. Figure 2b is the linear fitting of α_{eff} change with the number of Ir layers on top of the glass fiber. Linear fitting of these data gives a slope of 5.86×10^{-8} m^2 s^{-1}. Then the thermal conductivity of Ir layer can be calculated as 66.1 W m^{-1} K^{-1}. This value is much smaller than the thermal conductivity of bulk Ir 147 W m^{-1} K^{-1} at 313 K. The mechanism behind this reduction will be discussed later.

The total electrical resistance of Ir coating is calculated as Equation (3)

$$R_{\text{total}} = \frac{L}{A\sigma} = \frac{L}{Dn\delta_{\max}\sigma} \quad (3)$$

where σ and n $\delta_{\max}$ are electrical conductivity and total thickness of the layer on top of the glass fiber. It is evident in Equation (3) that electrical conductance $1/R_{\text{total}}$ changes with n linearly, and its slope is $D\delta_{\max}\sigma/L$. After five TET experiments, there are five groups data of (R^{-1}_{total}, n). Figure 2c shows linear fitting of the inverse of resistance against the number of Ir layers on top of the glass fiber. The fitted slope is 7.389×10^{-4} Ω^{-1}, and the electrical conductivity of Ir layer is calculated at 3.23×10^6 Ω^{-1} m^{-1}. This value is much smaller than the electrical conductivity of bulk Ir 18.81×10^6 Ω^{-1} m^{-1} at 313 K. The mechanism behind this reduction will be discussed later. From Figures 2b and c, it is clear that the effective thermal diffusivity and electrical conductance increases

NANO MICRO small

linearly with the number of Ir layers, verifying the assumption made earlier that each deposited film has the same electrical and thermal conductivities and ρc_p.

2.2. Thermal and Electrical Conduction in δ_{ave} = 0.6 nm Thick Ir Film

During film deposition, the process is controlled to yield a 1-nm coating thickness for monitoring inside the sputtering machine, giving δ_{max} = 1 nm and δ_{ave} = 0.6 nm for the Ir film. We have verified that the δ_{ave} = 0.6 nm Ir film is continuous as shown in Figure S1 (see Supporting Information). With regard to very thin films, like 0.6-nm thickness, the measurement used for the above film needs to be revised as the electric resistance of the δ_{ave} = 0.6 nm Ir layer is very large and instable, not suitable for direct TET measurement. In our measurement, if the electric resistance is larger than 20 kΩ, the noise will be very large, resulting in reduced measurement accuracy. So at the beginning of the experiment, a glass fiber of 407-μm length is first coated with a δ_{max} = 5 nm Ir film as the base layer, and a TET measurement is conducted. After that, a δ_{max} = 1 nm Ir layer is added every time as shown in **Figure 3**a. After six TET experiments, six different values of α_{eff} and electric resistance are obtained. It is evident, from the upper left inset of Figure 3a, that the normalized temperature rise versus time agrees very well between theoretical and experimental values. The measured effective thermal diffusivity has a modified relationship to the electrical conductance as $\alpha_{eff} = \alpha + L_{1,\,Lorenz}TL/(R_1 A_w \rho c_p) + L_{2,\,Lorenz}TL/(R_{2,n} A_w \rho c_p)$, where R_1 is the resistance of base layer (5-nm Ir coating) and $R_{2,n}$ (n = 1–5) is the resistance of n layers of δ_{max} = 1 nm Ir films, $L_{1,Lorenz}$ and $L_{2,Lorenz}$ are the Lorenz number of the base layer, and δ_{max} = 1 nm layer. Using the calculation for parallel resistors: $1/R_{total} = 1/R_1 + 1/R_{2,n}$ (n = 1–5, R_{total}: total resistance of the sample), we can determine $R_{2,n}$ easily. The slope of the fitting line is determined at 8.75×10^{-5} m^2 s^{-1} Ω (shown in Figure 3a). In the last five TET experiments the current is in a range of 154–194 μA to ensure a consistent temperature rise of the transient stage (≈11 K). The average temperature during the transient state is 309 K. With the same method for determining the Lorenz number of δ_{ave} = 6.4 nm Ir layer, we can obtain the Lorenz number of δ_{ave} = 0.6 nm Ir layer as 7.08×10^{-8} W Ω K^{-2}.

The effective thermal diffusivity of the whole sample is expressed as Equation (4)

$$\alpha_{\text{eff}} = \alpha_{\text{w}} + \frac{1}{(\rho c_p)_{\text{w}}} \frac{4\delta_{1,\max}}{\pi D}\left[k_1 - \alpha_{\text{w}}(\rho c_p)_{\text{c}}\right] + \frac{1}{(\rho c_p)_{\text{w}}} \frac{4n\delta_{2\,\max}}{\pi D}\left[k_2 - \alpha_{\text{w}}(\rho c_p)_{\text{c}}\right] \quad (4)$$

where $\delta_{1,max}$ is 5 nm and is for the first layer (base layer), k_1 is the thermal conductivity of the base layer, and k_2 is the thermal conductivity of a single δ_{max} = 1 nm Ir layer. In Equation (4), α_{eff} changes with n linearly as other parameters are constant for each round of measurement. With the same method used for the 6.4-nm thick Ir layer, we linearly fit the results for α_{eff} and inverse of total electrical resistance against n as shown in Figures 3b and c. The slopes of the fitting lines are determined to be 6.5×10^{-9} m^2 s^{-1} and 7.8×10^{-5} Ω^{-1}, respectively. Then the thermal conductivity and electrical conductivity of 0.6 nm thick Ir layer are calculated as 73.1 W m^{-1} K^{-1} and 3.46×10^6 Ω^{-1} m^{-1}, respectively. These values are much smaller than the thermal conductivity and electrical conductivity of bulk Ir 147 W m^{-1} K^{-1} and 19.07×10^6 Ω^{-1} m^{-1} at 309 K.

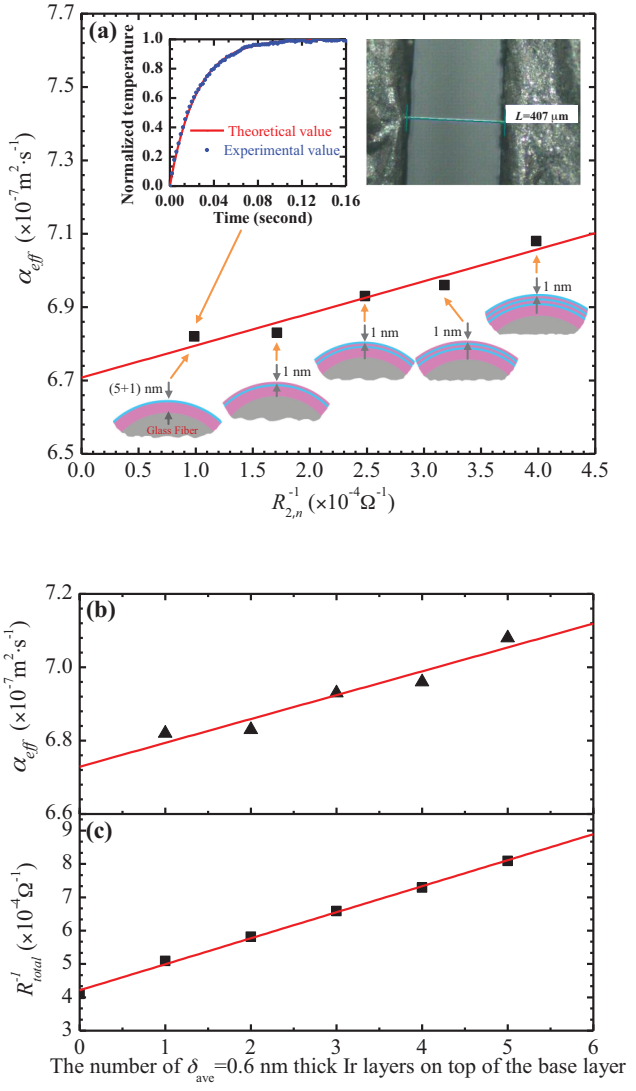

Figure 3. a) Variation of the effective thermal diffusivity of Ir-coated glass fiber (407 μm long) against the inverse of the electrical resistance for 0.6-nm Ir layers on top of the base layer. The solid line is a linear fit of the five data points. The upper left inset shows comparison between the theoretical fitting and experimental data for the normalized temperature rise for one 0.6-nm Ir layer on top of the base layer case. The upper right inset shows the Ir-coated glass fiber connected between two electrodes for TET measurement. b) Linear fitting of the effective thermal diffusivity change with the number of 0.6 nm Ir layers on top of the base layer. c) Linear fitting of the inverse of resistance change with the number of 0.6-nm thick Ir layers on top of the base layer. Dots are the experimental results, and solid lines are the linear fits.

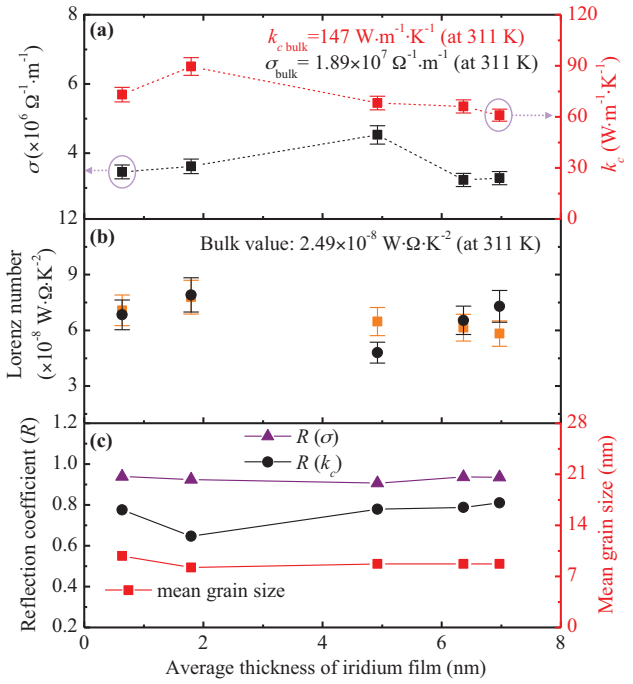

Figure 4. a) δ_{ave}-dependent electrical and thermal conductivity of Ir films. b) Lorenz number variation against thickness of Ir films. The squares are for data calculated from $L_{Lorenz} = A_w(\rho c_p)\psi/TL$ and circles are for data calculated from $L_{Lorenz} = k_c/\sigma T$. c) δ_{ave}-dependent electron reflection coefficient R at grain boundaries for the electrical conductivity and thermal conductivity. Also shown is the measured grain size based on X-ray diffraction (XRD).

2.3. Effect of Film Thickness on Thermal and Electrical Conduction in Ir Films

We have measured Lorenz number, electrical conductivity, thermal conductivity, and mean grain size of Ir films/layers with the average thickness of 0.6, 1.8, 4.9, 6.4, and 7 nm (corresponding to δ_{max} = 1, 2.8, 7.7, 10, and 11 nm). The results are shown in **Figure 4**. The uncertainty of measured thermal and electrical conductivities is estimated to be less than 5.9%, and the measurement errors in the Lorenz numbers are less than 12%. As can be seen from Figure 4a, both the electrical and thermal conductivities of the Ir films are significantly smaller than the corresponding bulk values. The average conductivity data for these films are reduced by 81% (electrical) and 51.2% (thermal) compared to bulk values at 311 K. No clear trend is observed for the thermal and electrical conductivity change with the film thickness. The electrical conductivity of 4.9-nm and 6.4-nm thick Ir are the biggest and smallest out of all the samples, which are 23.9% and 17.1% of the bulk value. But the thermal conductivity of 1.8-nm and 7-nm thick Ir are the highest and lowest out of all the samples, at 61.1% and 41.6% of the bulk value. It is evident that the electrical conductivity reduction is much bigger than the thermal conductivity reduction, which will lead to violation of the WF law. In the WF law, the Lorenz number is defined as $L_{Lorenz} = k_c/\sigma T$, and is 2.49 × 10^{-8} W Ω K^{-2}[[24]] for bulk Ir at room temperature. In Figure 4b squares are for Lorenz numbers calculated from $L_{Lorenz} = A_w\rho c_p\psi/TL$, and circles are for data directly calculated from the determined thermal and electrical conductivities as $L_{Lorenz} = k_c/\sigma T$. These two methods yield quite close results for the Lorenz number. The largest Lorenz number is about 7.8 × 10^{-8} W Ω K^{-2} for 1.8-nm thick Ir film, which is more than three times the bulk value. The smallest Lorenz number calculated from $L_{Lorenz} = A_w\rho c_p\psi/TL$ is 5.83 × 10^{-8} W Ω K^{-2} for the 7-nm Ir film. From $L_{Lorenz} = k_c/\sigma T$ the smallest one is 4.8 × 10^{-8} W Ω K^{-2} for the 4.9-nm Ir film. Both of these values are much bigger than the bulk value.

Yoneoka et al.[3] have measured electrical and thermal conductivities of free-standing Pt films formed by atomic layer deposition (ALD). The average Lorenz number is 3.82 × 10^{-8}, 2.79 × 10^{-8}, and 2.99 × 10^{-8} W Ω K^{-2} for 7.3-, 9.8-, and 12.1-nm Pt films, respectively. Conductivity data for the 7.3-nm Pt film are reduced by 77.8% (electrical) and 66.3% (thermal) compared to bulk values due to electron scattering at material and grain boundaries. The measurement results indicate that contribution of phonon conduction is significant in the total thermal conductivity of the ALD films. Experimental results of Zhang and co-workers[16,17] showed that the Lorenz numbers are around 7.0 × 10^{-8} and 5.0 × 10^{-8} W Ω K^{-2} for 21–37-nm and 53-nm polycrystalline Au films. Zhang and co-workers[4,5,17] used electron-beam (EB) lithography, EB physical vapor deposition (EBPVD) and isotropic/anisotropic-etching techniques to fabricate suspended Pt nanofilms; they found that the in-plane thermal conductivity was less than half of the corresponding bulk value and the nanofilm had significantly lower electrically conductive capacity than bulk platinum. The Lorenz numbers for the 15-, 28-, and 48-nm Pt nanofilms are several times over the bulk value; this deviation from the bulk value is due to the effect of grain-boundary scattering. Furthermore, their experimental results indicate that the grain-boundary scattering effect imposes greater influence on the charge transport than on the heat transport, similar to the results of this work. It should be pointed out that for very thin films, 5 nm or thinner, no research has been done, while such research is very critical to understand the effect of electrons scattering on thermal and electrical conduction. Herein, for the thinnest film we measured (δ_{ave} = 0.6 nm thick), the Lorenz number is 7.08 × 10^{-8} and 6.84 × 10^{-8} W Ω K^{-2} determined from $L_{Lorenz} = A_w\rho c_p\psi/TL$ and $L_{Lorenz} = k_c/\sigma T$, respectively.

From Figure 4a, we can see that the electrical conductivity of Ir keeps almost constant with the increase of the film thickness from 0.6 to 7 nm. The electrical conductivity is mainly determined by structure and nanograins of Ir films. The thermal conductivity shows a small reduction with increased thickness. To explore the mechanism behind this significant reduction of thermal and electrical conductivities discussed above, the Mayadas-Shatzkes (MS) model[19,20] is used to understand the strong electron scattering in the nanofilms. Based on the MS model, σ_f/σ_0 can be approximated by Equation (5)[25]

$$\frac{\sigma_f}{\sigma_0} = \left[1 + \frac{3(1-p)}{8k_0} + \frac{7}{5}\alpha\right]^{-1} \quad (5)$$

within 9% error when the film thickness and the grain diameter are not too small compared with the electron mean free

NANO MICRO small

path, i.e., α<10 and k_0>0.1. Here $\alpha = l_0R/d(1\text{-}R)$, $k_0 = \delta_{ave}/l_0$, σ_f and σ_0 are film and bulk electrical conductivities, R is the electron reflection coefficient at grain boundaries, p the specular reflection parameter of electrons at film surfaces, δ_{ave} the average film thickness, l_0 electron mean free path, and d the average grain size. The MS model is for a film structure in which the grains are columnar, with the column axis normal to the film plane. This structure is generally true for films deposited by evaporation or sputtering. Our X-ray diffraction (XRD) study (Figure S3 in Supporting Information) tells us that the grain size is usually comparable to or larger than the film thickness, which supports the columnar grain structure in our case. The value of p is 1 because thermal and electrical conductivities of Ir film change little with the increase of the average thickness from 0.6 to 7 nm, which indicates a weak effect of the film thickness. The electrical conductivity σ_0 can be calculated from $L_{Lorenz} = k_c/\sigma T$ and the Lorenz number of bulk Ir is 2.49×10^{-8} W Ω K^{-2} from 273 to 373 K.[24] There are two unknown parameters in Equation (5): l_0 and R. The Fermi energy (E_F) of Ir is 0.761 Ry,[26] and its Fermi velocity can be calculated from $v_F = (2E_F/m_e)^{1/2}$; the value is 1.91×10^6 m s^{-1}. When temperatures are much lower than both the Debye temperature and the Fermi temperature, the heat capacity of metals with electronic contributions is $C = \gamma T$ where γ is 3.1 mJ mol^{-1} K^{-2}.[24] Then from the kinetic theory $k = Cv_Fl_0/3$,[24] the electron mean free path l_0 of Ir is calculated at 2.04 nm.

We choose the 0.6-nm thick Ir film as an example for analysis. The grain size was determined by using XRD to be 9.8 nm. For electrical conductivity, p is 1 and R is fitted to be 0.94 to make the theoretical prediction close to the experimental data. For thermal conductivity R is determined to be 0.78, based on the theoretical model. From Figure 4b, it is obvious that the Lorenz numbers calculated from the two methods are several times bigger than the Sommerfeld value of $L_0 = 2.49 \times 10^{-8}$ W Ω K^{-2}, which indicates that the grain-boundary scattering effect imposes greater influence on the charge transport than on the heat conduction. It is evident in Figure 4c that the reflection coefficient R for the electrical conductivity is much bigger than that for thermal conductivity, which indicates that the electron scatterings on the grain boundaries exert different influences on current and heat transport in the Ir films. For charge transport, only the electrons quantum mechanically passing through all the boundaries along the background scattering can contribute to the measured electrical conductivity. However, for thermal transport, the scenario becomes different. Those electrons reflected from grain boundaries could have energy exchange with the local phonon, thereby leading to thermal transport in space though they have no charge transport contribution. Therefore, the fitted smaller value of R for thermal transport reflects this phenomenon. For the 0.6-nm Ir film case, based on the R values of 0.94 for charge transport and 0.78 for heat conduction, to a first-order estimate, it is conclusive that electrons reflected from grain boundaries have about 17% of their energy exchanged with phonons at grain boundaries. It is found that electron reflection at grain boundaries can be 90% or higher. The nominal electron reflectance for thermal conduction at grain boundaries does not show a clear trend with the film thickness, and is pretty much constant with respect to film thickness, except for the visibly lower value for the 1.8-nm-thick Ir film. As demonstrated here, grain-boundary electron scattering greatly reduces the thermal and electrical conductivities due to the very small grain in these ultrathin films.[19] The total thermal conductivity of metallic film is the sum of electron thermal conductivity k_e and phonon contribution k_{ph}. In bulk metal, at room temperature electrons have about 90% – 95% contribution to the total thermal conductivity, and phonons only have about 5% – 10%,[27] so in bulk Ir the phonon's contribution $k_{ph,\,bulk}$ is less than 14.7 W m^{-1} K^{-1}. In the ultrathin Ir films studied here, phonons' contribution to the total thermal conductivity $k_{ph,\,film}$ is smaller than in bulk Ir $k_{ph,\,bulk}$ owing to the extensive nanograins in the film. Therefore, it can be concluded that in the Ir films studied here, phonon thermal conductivity k_{ph} is less than 14.7 W m^{-1} K^{-1}. Herein, the average thermal conductivity of Ir film from 0.6 – 7 nm thick is more than 60 W m^{-1} K^{-1}. It is clear that electron thermal transport is still dominant in these films. We have studied the grain structure using high-resolution transmission electron microscope (TEM) as shown in Figure S2 (See the Supporting Information). The crystallographic orientation varies from grain to grain, gives rise to orientation mismatch at grain boundaries. Such orientation mismatch plays a big role in the electron scattering and reflection described above.

3. Discussion on Characterization Capacity and Uncertainty

Herein, the thinnest film measured is 0.6 nm. This limitation is imposed by the sample preparation process, not by the characterization technique itself. Based on the data reported herein, we conclude it is possible to characterize the thermal conduction in even thinner films, like sub-0.5-nm thickness. For such measurement, instead of a glass fiber, a dielectric fiber (e.g., polymer) with a lower thermal conductivity and smaller diameter (only a few micrometers) will help improve the measurement accuracy. The layer-by-layer addition technology used in this work measures the thermal conduction in ultrathin films of which the top is a free surface and the bottom is next to another metallic film. However, it is feasible to study the thermal conduction of ultrathin films whose bottom is next to another different material, either dielectric or metallic. This method will provide an unprecedented way to explore electron scattering at different material interfaces.

During our TET characterization, the experiment is conducted in a vacuum chamber maintained at 30 mTorr. The small effect from pressure on the measured thermal diffusivity ($\Delta\alpha_p$) has very little influence on the data analysis. This lack of influence is because in the linear fitting used in the experiment, only the thermal diffusivity increase/change with the film electrical conductance or film thickness is used. In our experiment, the radiation effect exists for all cases. Increase of the film thickness on the glass fiber will change the radiation from one side since a thicker metallic layer shields more radiation from the fiber surface. Glass has an emissivity of 0.92 at room temperature. For the 0.6-nm Ir film

case, total change of the film thickness from $\delta_{max} = 6$ to 10 nm will change the radiation emissivity from the sample by less than 0.07, to a first-order estimate. This change will give a total thermal diffusivity change of 2.0×10^{-9} m^2 s^{-1}.

In the experiment, different currents are tried for each sample, and the case that gives nearly the same temperature rise of the sample is taken for data processing to determine the thermal diffusivity. The effect of the slight nonuniform and nonconstant heating with the resistance change can be expressed as $-\varepsilon I^2 RL/(A_c \pi^2 \rho c_p)$ where ε is the temperature coefficient of the sample's electrical resistance, and I is the electrical current. In our experiment, the resistance increase by heating is controlled to be around 2% or less. Therefore, the thermal diffusivity change by this nonconstant and nonuniform heating is less than 2×10^{-13} m^2 s^{-1}, which is negligible for the experiments. Separate experiments have been conducted to evaluate the electrical contact resistance using the four-probe method. For glass fibers coated with Ir, silver paste does a good job in securing the contact between the wire and the electrodes with a contact resistance of only a few ohms. Since the glass fiber has a low thermal conductivity, any potential thermal contact resistance between the wire and the base will become negligible compared with the thermal resistance of the sample itself. Also in our experiment, since only the change of the thermal diffusivity and electrical resistance accounts in the linear data fitting, the electrical and thermal contact resistances will remain the same for one sample with different layers of the film, and will have negligible effect on the final results.

During TET measurement, in the cross-sectional direction of the sample, the characteristic thermal diffusion time is $\Delta t_1 \approx r^2/\alpha$ (r is the wire radius) and in the length direction the characteristic thermal diffusion time is $\Delta t_2 \approx 0.2026 L^2/\alpha$. In the case of single-layer 6.4-nm Ir on the glass fiber (401 μm long as shown in Figure 2), Δt_1 is estimated to be about 30 μs and Δt_2 is about 0.06 s. It is obvious $\Delta t_1 << \Delta t_2$. So during the relative long-time temperature evolution of the wire in TET measurement, the heat conduction in the cross-section quickly reaches its equilibrium and the temperature distribution across the glass fiber's cross-section is very uniform. The estimated average temperature rise of the sample during the transient TET stage is around 10–16 K. In the past, we have calibrated the temperature coefficient of electrical resistance for sputtering coated gold on TiO_2 wire over a very large temperature range (>60 K).[28] The electrical resistance changes with temperature linearly, and the nonlinear effect is estimated to be negligible, and will affect our results to a very limited extent.

All experimental devices and equipment, such as the constant current source, oscilloscope and digital multimeter are calibrated before the measurement. Therefore the uncertainties from current and resistance readings are negligible. As for the coating thickness, it has ±0.1 nm uncertainty from the coating machine. The TET experiment has an uncertainty of fitting and repeatability better than 2.5%.

4. Conclusion

In summary, the thermal and electrical conductivities (k and σ) of Ir films with average thickness from 7 nm down to 0.6 nm were characterized by the TET method. The results showed that k and σ of Ir films can be reduced by more than 59% and 82% compared to bulk Ir. A much stronger reduction in σ significantly increased the Lorenz number to around $6 - 8 \times 10^{-8}$ W Ω K^{-2} or larger, close to a twofold increase of the bulk value. k, σ, and L_{Lorenz} values of the Ir films showed little variation with thickness from 0.6 to 7 nm, which reflects a weak effect from surface electron scattering (film thickness) and more from grain-boundary scattering/reflection. For electrical conduction, electron reflection at grain boundaries is 90% or higher.

5. Experimental Section

The TET technique has been proved to be an effective, accurate, and fast approach to measuring the thermal diffusivity of one-dimensional solid materials. The measurement accuracy of this technique has been fully examined by characterizing reference materials, both metallic and dielectric. The TET measurement gives results agreeing with reference values with less than 5% difference. The TET technique has been used extensively in our lab to measure the thermal diffusivity/conductivity of nonconductive materials by coating the sample with a very thin metallic film (e.g., gold). Guo et al. have used this technique to measure the thermal diffusivity of microscale polyester fibers[21] and micro/nanoscale polyacrylonitrile fibers.[29] Furthermore, Feng et al. employed the TET technique to measure the thermal diffusivity of thin films composed of anatase TiO_2 nanofibers,[28] single anatase TiO_2 nanowires[30] and free-standing micrometer-thick poly(3-hexylthiophene) films.[31] Sound agreements have been obtained between the measured thermal diffusivities and reference values. Huang et al.[32] extended the TET technique and measured thermophysical properties of multiwalled carbon nanotube bundles at elevated temperatures up to 830 K.

A schematic of the TET technology is presented in Figure 1b to demonstrate how this technique can be used to characterize the thermal transport in one-dimensional micro/nanostructures. At the beginning of the experiment, the to-be-measured wire is suspended between two aluminum electrodes. In the experiment, to enhance the electrical and thermal contact of the sample to electrode, silver paste is applied at the contact point. The sample is placed in a vacuum chamber to suppress the effect of gas conduction during measurement. During thermal characterization, a step DC current is fed through the wire to generate electric heat. In the experiment, the electrical current should be chosen carefully to make sure the temperature rise of all the TET experiments is almost identical for the sample glass fiber. The temperature evolution of the wire is determined by two competing processes: one is joule heating by the electrical current, and the other one is the heat conduction along the wire to electrodes. The temperature change of the wire will induce an electrical resistance change, which leads to an overall voltage change of the wire. Therefore the voltage change of the wire can be used to monitor its temperature evolution. A typical V–t profile recorded by the oscilloscope is shown in Figure 1c. As explained in this figure, under the feeding of a square current, the induced voltage profile (red solid line) undergoes a rapid increase phase and then reaches the steady state, which means that heat transfer equilibrium is established. The transient phase reflects the resistance change of the wire, which

NANO MICRO small

in turn gives an idea of how quickly/slowly the temperature of the wire evolves. This temperature change is strongly determined by the thermophysical properties of the wire. A higher thermal diffusivity of the wire will lead to a faster temperature evolution, which means a shorter time to reach the steady state. Therefore, the transient voltage/temperature change can be used to determine the thermal diffusivity. When determining thermal diffusivity of the sample, no real temperature rise is needed. In fact, only the normalized temperature rise based on the voltage increase is needed. More details can be found in Feng's work.[31]

During TET thermal characterization, the sample's voltage evolution (V_{sample}) recorded by the oscilloscope is directly related to the average temperature change of the sample as Equation (6)

$$V_{sample} = I R_0 + I \eta \frac{8 q_0 L^2}{k \pi^4} \times \sum_{m=1}^{\infty} \frac{1 - \exp\left[-(2m-1)^2 \pi^2 \alpha t / L^2\right]}{(2m-1)^4} \quad (6)$$

where V_{sample} is the recorded overall voltage of the sample, I is the constant current fed through the sample, R_0 the resistance of the sample before heating, η the temperature coefficient of resistance of the sample, q_0 the electrical heating power per unit volume, and k the thermal conductivity of the sample. It is explicit that the measured voltage change is inherently related to the temperature change of the glass fiber. The normalized temperature rise T^*_{exp} based on the experimental data can be calculated as $T^*_{exp} = (V_{sample} - V_0)/(V_1 - V_0)$, where V_0 and V_1 are the initial and final voltages across the sample (as illustrated in Figure 1c).

The theoretical normalized temperature rise (T^*) is solved for a one-dimensional heat transfer problem and is expressed as in Equation (7)

$$T^* = \frac{96}{\pi^4} \sum_{m=1}^{\infty} \frac{1 - \exp\left[-(2m-1)^2 \pi^2 \alpha t / L^2\right]}{(2m-1)^4} \quad (7)$$

where α and L are thermal diffusivity and length of the sample, respectively. In our work, after T^*_{exp} is obtained, different trial values of α are used to calculate the theoretical temperature rise based on Equation (7) and fit the experimental results (T^*_{exp}). The value that gives the best fit of T^*_{exp} is taken as the thermal diffusivity of the sample.

Scanning electron microscopy (SEM) was employed to measure the diameter of glass fibers and one of the sample images is presented in the lower right inset of Figure 2a. The diameter of glass fibers is measured at 9.17 ± 0.54 μm. The masses of three groups of glass fibers were measured using a microbalance. Detailed information about the three groups of the glass fibers such as number of fibers, diameter, length and mass is listed in **Table 1**.

Table 1. Details of density evaluation for glass fiber

Sample index	Number of fibers in the bundle	Length [mm]	Mass [mg]	Density [kg m^{-3}]	Average Density [kg m^{-3}]
1	23	348.996	1.1	2077	2070 ± 121
2	39	301.625	1.6	2061	
3	39	600.075	3.2	2072	

As number, diameter, length, and mass are known, the density can be calculated. The average density is 2070 ± 121 kg m^{-3}, and the specific heat value used in the calculation is 745 J kg^{-1} K^{-1}.[22]

For our study of Ir nanofilms, the glass fiber is coated with Ir by using a sputtering machine Quorum Q150T S from Quorum Technologies Company. Figure S2 shows the high-resolution TEM images of iridium films coated on copper grids with carbon film. It is observed that the iridium films have good crystallinity and they are nanocrystalline material. The thicknesses δ_{max} (shown in Figure 1d; 1, 2.8, 7.7, 10, and 11 nm) of the Ir film were monitored during deposition using a quartz crystal microbalance. To assure accuracy, the thickness was also verified by using a silicon wafer coated with the same thickness Ir. The coated silicon wafer was scanned using an atomic force microscope (AFM) and the thickness reading from the Quorum Q150T S was found to be accurate.

As shown in Figure 1d, the vapor deposition only coats the top side of the glass fiber and the thickest portion (δ_{max}) is on the center top of the glass fiber because during the coating process the glass fiber is stationary, not rotated as in normal sample coating. The glass fiber itself is very small in comparison with the whole deposition plume in the sputtering chamber. Therefore it is physically reasonable to assume the metal-atom vapor deposits on the glass fiber as shown in Figure 1d, just like snow precipitation on a horizontal cylinder. The thickness (δ_θ) of the metallic layer varies with the location on the fiber surface as: $\delta_\theta = \delta_{max}\cos\theta$ (illustrated in Figure 1d), where θ is the angle from the vertical direction. The cross-sectional area of the metallic coating can be expressed as $A_c = 2\int_0^{\frac{\pi}{2}} \cos\theta \cdot \delta_{max} \cdot r \cdot d\theta = D \cdot \delta_{max}$ and its average thickness is $\delta_{ave} = 2\delta_{max}/\pi$. In this work, we use δ_{ave} as the characteristic value to describe the thickness of the coating under study. For the scenario where the first layer has the same thickness as the layers added later ($\delta_1 = \delta_2$), if deposition has been done n times, the total average thickness of the film would be $\Delta z = n\ \delta_{ave} = 2n\ \delta_{max}/\pi$, where δ_{ave} is the average thickness of each layer. The cross-sectional area of the coating (A_c) is $D\ n\ \delta_{max}$, where D is the diameter of glass fiber. If the first layer thickness δ_1 is different from δ_2 (for extremely thin films), after we add n layers of films of δ_2 thickness, we would have $\Delta z = \delta_{1,ave} + n\ \delta_{2,ave}$, and $A_c = D \times (\delta_{1,max} + n\ \delta_{2,max})$. The terms $\delta_{1,ave}$, $\delta_{1,max}$, $\delta_{2,ave}$, and $\delta_{2,max}$ are the average and maximum thicknesses of the first layer and the layers added later.

Supporting Information

Supporting Information is available from the Wiley Online Library or from the author.

Acknowledgements

Support of this work from the Office of Naval Research (N000141210603), Army Research Office (W911NF-12-1-0272), and National Science Foundation (CBET-0931290) is gratefully acknowledged. We are grateful to MO-SCI Corporation for providing the glass-fiber samples used in this work. H. L. is supported by the China Scholarship Council for a two-year placement at Iowa State University. N. M. thanks the National Natural Science Foundation

of China (NSFC: 51076146) for support. X. W thanks the Eastern Scholar Program of Shanghai, China for support.

[1] L. A. Moraga, A. Vilche, *Thin Solid Films* **1976**, *38*, 117–130.
[2] M. Tay, K. B. Li. , Y. H. Wu, *J. Vac. Sci. Technol. B* **2005**, *23*, 1412–1416.
[3] S. Yoneoka, J. Lee, M. Liger, G. Yama, T. Kodama, M. Gunji, J. Provine, R. T. Howe, K. E. Goodson, T. W. Kennyt, *Nano Lett.* **2012**, *12*, 683–686.
[4] X.Zhang, H. Q. Xie, M. Fujii, H. Ago, K. Takahashi, T. Ikuta, H. Abe, T. Shimizu, *Appl. Phys. Lett.* **2005**, *86*, 171912.
[5] X. Zhang, Q. G. Zhang, B. Y. Cao, M. Fujii, K. Takahashi, T. Ikuta, *Chin. Phys. Lett.* **2006**, *23*, 936–938.
[6] S. P. Gurrum, W. P. King, Y. K. Joshi, K. Ramakrishna, *J. Heat Trans.-T. ASME* **2008**, *130*, 082403.
[7] K. Fuchs, *Proc. Cambridge Philos. Soc.* **1938**, *34*, 100–108.
[8] E. H. Sondheimer, *Adv. Phys.* **1952**, *1*, 1–42.
[9] S. B. Soffer, *J. Appl. Phys.* **1967**, *38*, 1710–1715.
[10] Y. Namba, *Jpn. J. Appl. Phys.* **1970**, *9*, 1326–1329.
[11] S. P. Gurrum, Y. K. Joshi, W. P. King, K. Ramakrishna, *IEEE Electr. Device L* **2004**, *25*, 696–698.
[12] P. Nath, K. L. Chopra, *Thin Solid Films* **1974**, *20*, 53–62.
[13] I. S. Beloborodov, A. V. Lopatin, F. W. J. Hekking, R. Fazio, V. M.Vinokur, *Europhys. Lett.* **2005**, *69*, 435–441.
[14] N. Stojanovic, D. H. S. Maithripala, J. M. Berg, M. Holtz, *Phys. Rev. B* **2010**, *82*, 075418.
[15] V. Tripathi, Y. L. Loh, *Phys. Rev. Lett.* **2006**, *96*, 046805.
[16] Q. G. Zhang, B. Y. Cao, X. Zhang, M. Fujii, K.Takahashi, *Phys. Rev. B* **2006**, *74*, 134109.
[17] H. D. Wang, J. H. Liu, X. Zhang, Z. Y. Guo, K. Takahashi, *Heat Mass Transfer* **2011**, *47*, 893–898.
[18] M. N. Ou, T. J. Yang, S. R. Harutyunyan, Y. Y. Chen, C. D. Chen, S. J. Lai, *Appl. Phys. Lett.* **2008**, *92*, 063101.
[19] A. F. Mayadas, M. Shatzkes, *Phys. Rev. B* **1970**, *1*, 1382–1389.
[20] A. F. Mayadas, M. Shatzkes, J. F. Janak, *Appl. Phys. Lett.* **1969**, *14*, 345–347.
[21] J. Q. Guo, X. W. Wang, T. Wang, *J. Appl. Phys.* **2007**, *101*, 063537.
[22] F. P. Incropera, D. P. DeWitt, *Fundamentals of heat and mass transfer*, 5th ed., John Wiley and Sons, New York, **2002**, pp. 934.
[23] X. W. Wang, X. F. Xu, S. U. S. Choi, *J. Thermophys. Heat Transfer* **1999**, *13*, 474–480.
[24] C. Kittel, *Introduction to solid state physics*, 5th ed., Wiley, New York, **1976**, pp. 143–178.
[25] T. Q. Qiu, C. L. Tien, *J. Heat Trans.-T ASME* **1993**, *115*, 842–847.
[26] O. K. Andersen, A. R. Mackintosh, *Solid State Commun.* **1968**, *6*, 285–290.
[27] R. Fletcher, D. Greig, *Philos. Mag.* **1967**, *16*, 303–315.
[28] X. Feng, X. Wang, X. Chen, Y. Yue, *Acta Mater.* **2011**, *59*, 1934–1944.
[29] J. Q. Guo, X. W. Wang, L. J. Zhang, T. Wang, *Appl. Phys. A* **2007**, *89*, 153–156.
[30] X. H. Feng, X. P. Huang, X. W. Wang, *Nanotechnology* **2012**, *23*, 185701.
[31] X. H. Feng, X. W. Wang, *Thin Solid Films* **2011**, *519*, 5700–5705.
[32] X. P. Huang, J. M. Wang, G. Eres, X. W. Wang, *Carbon* **2011**, *49*, 1680–1691.

Received: November 19, 2012
Revised: December 28, 2012
Published online: February 22, 2013

